2011 IEEE/RSJ International Conference on
Intelligent Robots and Systems
September 25-30, 2011. San Francisco, CA, USA

A Lizard-Inspired Active Tail Enables Rapid Maneuvers and Dynamic Stabilization in a Terrestrial Robot

Evan Chang-Siu†, Thomas Libby†, Masayoshi Tomizuka†, and Robert J. Full‡

***Abstract*— We present a novel approach to stabilizing rapid locomotion in mobile terrestrial robots inspired by the tail function of lizards. We built a $177\ (g)$ robot with inertial sensors and a single degree-of-freedom active tail. By utilizing both contact forces and zero net angular momentum maneuvering, our tailed robot can rapidly right itself in a fall, avoid flipping over after a large perturbation, and smoothly transition between surfaces of different slopes. We also use a modeling approach to show that a tail-like design offers significant advantages to other alternatives, including reaction wheels, when the speed of response is important.**

I. INTRODUCTION

Robots can drive [1] with treads, run [2], [3] with legs, and climb [4], [5], [6] with adhesive pads over a variety of challenging surfaces, but in making fast, stable transitions they still lag far behind animals. These robots have fast, stable steady-state dynamics, even in the face of rough terrain. However, this is often due to carefully tuned passive dynamics, rather than feedback control [2]. Large perturbations can push a robot outside the basin of stability of these mechanisms, leading to catastrophic failure. To approach the robust behaviors of fast terrestrial animals, robots must be capable of rapid, sensory-driven feedback control.

A major difficulty for executing such control is that ground contact forces in rough terrain may be unpredictable or unavailable due to missed footholds, slippery substrates or unanticipated aerial phases. Recent studies in lizards have revealed a potentially elegant solution: they use their tails for stability, rapid reorientation, and perturbation recovery [7], [8], either through direct contact with the surface, or through zero net angular momentum maneuvers, similar to the well-known righting of a falling cat [9], [10], or of tumbling gymnasts [11], [12]. In both cases, attitude control is relatively simplified - torque applied through the tail yields an instantaneous, predictable counter-torque on the body. The result is remarkable performance for a terrestrial animal - geckos can right themselves in $0.106\ (s)$, effect large changes in pitch, roll, and yaw while mid air, and climb up a vertical wall at over 15 body lengths per second [7], [13].

We were inspired by the robust transition behavior of agama lizards to examine whether an active tail could expand the performance of a terrestrial robot. Figure 1 shows an agama performing a rapid transition over a low-friction substrate. When the feet slip during the jump, the perturbation in ground reaction forces generates angular momentum, which causes the animal to tumble forward through the air. Unchecked, this momentum would rotate the lizard's body outside of the range where it could safely land on the wall. To prevent the body from rotating, the animal rapidly swings its tail towards its head, transferring momentum from one link to the other. This behavior enables a significantly higher success rate than would be predicted for animals without a tail [8].

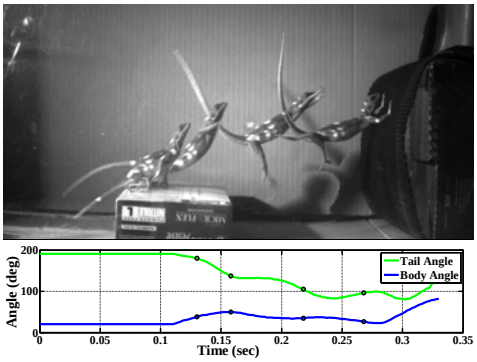

Fig. 1. Overlay plot of a lizard jumping off a low-friction surface. Note the use of tail indicated by the green line during flight, the near constant body angle indicated by the blue line, and the successful landing on the wall.

Zero net angular momentum control has been extensively proposed in space robots and satellites, for both attitude control and manipulation [14], [15], [16], and reaction wheels have been employed for fine direction control in satellites [17]. Other robots have employed angular momentum for brachiation [18], hopping [19], and for landing control [20], [21]. Momentum-based control has appeared in terrestrial vehicles for zero-speed bicycle stabilization [22], [23], and

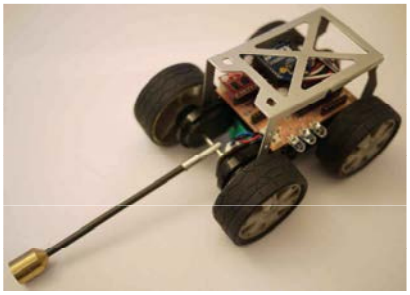

Fig. 2. *Tailbot*, prototype of tailed car.

This work was supported by the NSF CiBER-IGERT under Award DGE-0903711 and the United States Army Research Laboratory under the Micro Autonomous Science and Technology Collaborative Technology Alliance.

Corresponding author: evancs@berkeley.edu † Department of Mechanical Engineering, University of California Berkeley, Berkeley ‡ Department of Integrative Biology, University of California Berkeley, Berkeley

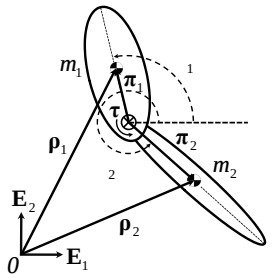

Fig. 3. Diagram of two link planar model for aerial reorientation.

has been implemented in a small robotic bicycle [24]. Recent robots have incorporated simple tails for stability in climbing [4], [5], and in a robot that runs on water [25]. These tails rely on passive substrate contact, but could be easily adapted to add the capability we show here. We hypothesize that we can greatly expand the basin of stability for dynamic locomotion by supplementing terrestrial robots with an actuated tail-like limb capable of both contact- and inertial-based torque inputs.

As a first step toward capturing the incredible mobility of natural tails, we examined the capability of a single degree-of-freedom (DOF) tail to stabilize planar dynamic tasks by creating the first robot with a controllable active tail (Fig. 2). In this paper, we show that a simple active tail with a simple controller can enable rapid reorientation and recovery from large perturbations. Further, we show that a tail-like design has significant advantages over other similar mechanisms, including reaction wheels and back-bending.

II. Modeling and Analysis

A. Equations of Motion

To inform the design of our robot, we derived a planar two-link rigid body model for aerial reorientation with the absolute body and tail angles referenced to horizontal as shown in Fig. 3. The two bodies are joined by a pin, where relative torque, $= \mathbf{E}_3$, is provided by a DC motor at the pivot.

For ease of simulation, we developed a state space model of the system in the form

$$\dot{\mathbf{x}} = \mathbf{f}(\mathbf{x}) + \mathbf{g}(\mathbf{x})\mathbf{u} \tag{1}$$

where the states, $\mathbf{x} = [\ _1,\ \dot{}_1,\ _2,\ \dot{}_2]^T$, consist of the angular position and velocity of the links and the control input, $\mathbf{u} =$, is the relative torque.

Although the equations of motion can be derived using a Lagrangian or Hamiltonian formulation [26], the Newtonian formulation is used here for clarity. Without loss of generality, we assume that the center of mass (COM) of the system exists at the same location as the world fixed origin, *O*, in Fig. 3. This results in the constraint

$$m_1\ _1 + m_2\ _2 = \mathbf{0} \tag{2}$$

where $_i$ is the vector from the origin to the COM of each link and m_i is the mass of each link. The individual angular momenta for each link, $\mathbf{H}_{io}$, about the origin can then be defined as

$$\mathbf{H}_{io} = I_i\ _i + m_i\ _i \times \dot{}_i \tag{3}$$

where $_i = \dot{}_i\mathbf{E}_3$ is the angular velocity of each link and I_i is the moment of inertia (MOI) about the COM of each link. If it is assumed that no external forces or torques act on the system then the angular momentum is constant, its derivative, $\dot{\mathbf{H}}_o = \mathbf{0}$, and

$$\dot{\mathbf{H}}_{1o} = -\dot{\mathbf{H}}_{2o} \tag{4}$$

With this assumption the derivative of the second link's angular momenta, $\dot{\mathbf{H}}_{2o}$, is easily written from the derivative of the first links angular momenta

$$\dot{\mathbf{H}}_{1o} = \ +(\ _1 - \ _1) \times m_1 \ddot{}_1 \tag{5}$$

where $_i$ is the vector from the pivot to the COM of each link. By combining (2), (4), (5), and the derivative of (3) the fourth order nonlinear state space model in (1) can be formed. The details of $\mathbf{f}(\mathbf{x})$ and $\mathbf{g}(\mathbf{x})$ can be found in the Appendix.

B. Active Tail vs. Active Flywheel

Compared to the tail-like design we present here, disk-like inertial loads, [17], [24], are not limited in stroke. This is a clear advantage for momentum wheels in situations that demand large rotations of the body, or when angular momentum must be stored for long periods. However, disk-like mechanisms face reasonable limits on size; the diameter of the disk must be significantly less than the size of the vehicle. This makes it difficult to increase the MOI since MOI is quadratically dependent on length while only linearly dependent on mass. A tail could reasonably be several times the length of a robot; indeed lizards with tails over twice body length are common [27]. Hence, to achieve the same rotational impulse with comparable weight, a disk-like design will utilize small MOI and large angular velocity, while a tail-like design will use large MOI and low speed.

The negative effects of increased tail length are not immediately clear, but could include increased weight to maintain sufficient stiffness and decreased mobility. Spinning a disk to high speed requires relatively high mechanical power, generates vibration, and results in gyroscopic effects that may reduce maneuverability. Rotations in multiple axes would require multiple disks, or a compact mechanism to rotate a single disk to an arbitrary axis. Studies in gliding geckos have revealed that a single tail can effect rotations in all three axes with only two degrees of freedom [7]. The packaging flexibility afforded by tail-like inertial appendages can result in much larger inertia for the same weight.

We used our dynamic model to examine the relative performance of a flywheel design for our test platform over a range of reasonable masses and lengths. The COM of the flywheel was positioned at the COM of the vehicle body. We limited the maximum allowable diameter to fit within the dimensions of the robot. With comparable mass and tail

length/wheel radius, performance offered by the two geometries is nearly identical; differences are primarily due to the fact that the tail is not attached to the COM of the robot. However, the overall dimension (diameter) of the wheel must be twice the length of the tail for comparable performance. Practical applications would likely tolerate diameters of less than one half body length. Therefore, when the diameter of the disk is exactly half the length of the body and the mass of the disk is reasonably 10% of the body, from Fig. 4, it would take 0.066 (s) to rotate the body 45°. For a tailed design the length can be made arbitrarily long and for the case when the relative tail length is equivalent to body length then half of the previous rise time is achieved, 0.033 (s), as shown in Fig. 5. For the disk to acquire the same time performance its mass would have to be increased to twice the body mass.

Our model predicts that momentum wheels are ideal for applications where slow, precise adjustments are necessary, as in satellites or for static balancing. For rapid, dynamic adjustments of less than one half rotation, a tail can be more compact and significantly lighter. Tails have another significant advantage over momentum wheels for dynamic robots - the ability to contact the substrate and change the total angular momentum of the system. Geckos were observed using small motions of their tails to contact the substrate and prevent pitch-back during rapid climbing [13]. We found tail-substrate interaction in our robot to be beneficial, particularly in reducing the drawback of limited tail stroke.

Another proposed mechanism of zero net angular momentum maneuvering is exemplified in the well-known falling cat [9] and the robots and models which have followed its design, where back-bending is the primary source of internal momentum. Compared to a tail-like inertial mechanism, in back-bending, the two links are similar in mass and length, and appendages or wheels are mounted on both links. This mechanism enabled air-righting in a robot [28], though the response was significantly slower than that observed in lizards. As observed by [28], the primary disadvantage is that in this case the orientation of the second link is also important; this constrains the performance of reorientation and makes pitch adjustments like those we show here impossible.

III. Robot Design

A. Mobile Robot Platform

To explore the effects of adding an active tail to an existing robot, we modified a small terrestrial vehicle in the form of a commercial radio-controlled car (*FlipZ, Radio Shack*). The car was designed with two independent DC motors to drive the left and right sets of wheels. We reconfigured the gear trains such that one motor drove the front wheels, while the other drove a single revolute joint at the rear, onto which we secured a 5/32" (0.397 (cm)) diameter carbon fiber tube and brass tip. The total tail stroke available was 255° beginning at 70° between the body and tail when fully pitched up as shown in Fig. 6. We measured the moment of inertia for the body and tail following the pendulum method in [29]. The final parameters of the robot are listed in Table I.

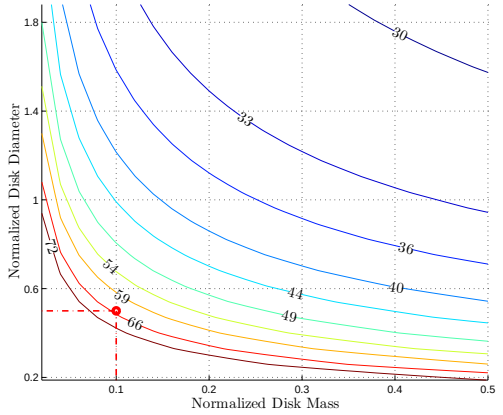

Fig. 4. Contour plot of time in milliseconds for the body to rotate 45° using a *disk* design with disk mass and diameter normalized against body mass and length respectively. The red dot indicates the rise time when the relative mass of the tail is 10% and the diameter of wheel is half the length of the body. As relative disk mass and length increase, time decreases.

The preexisting control circuitry was replaced with custom electronics that included a microcontroller (*Arduino*, pro-mini, 3.3 (V), 8 (MHz)), a motor driver (*Pololu* FNG-6612), a three-axis accelerometer (*Analog Devices*, ADXL345, ±2 $(gees)$) and gyroscope (*Invensense*, IDG-3200, ±2000 $(°/s)$), wireless communication module (*Xbee*), and LED indicator lights for timing and visualizing control effort. The robot was powered with two lithium polymer

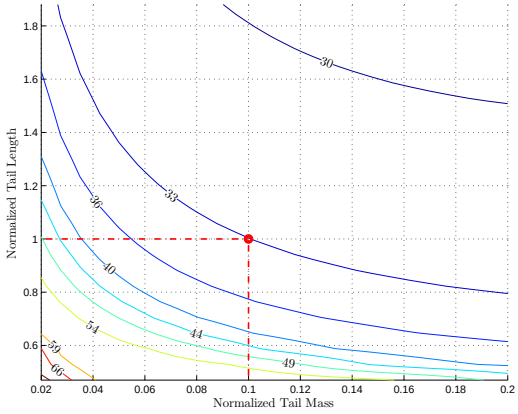

Fig. 5. Contour plot of time in milliseconds for the body to rotate 45° using a *tail* design with tail mass and length normalized against body mass and length respectively. The red dot indicates the rise time when the relative mass of the tail is 10% and the length of tail is equal to the length of the body. As relative tail mass and length increase, time decreases.

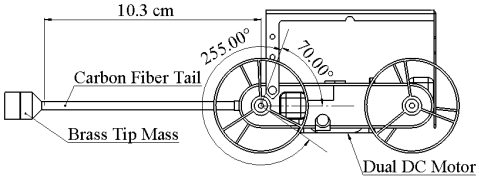

Fig. 6. Side view of *Tailbot* displaying the motor location, tail design, and tail stroke. The specified distance between the COM of the tip mass to center of the pivot is 10.3 (cm).

TABLE I

Tailbot MEASUREMENTS.

Parameter	Value
overall size	$2.8\times10^{-1}\ \times\ 9.3\times10^{-2}\ \times\ 7.0\times10^{-2}\ (m)$
stall torque	$5.0\times10^{-3}\ (Nm)$
no load ang. vel.	$5.4\times10^{3}\ (rad/s)$
gear ratio	$17.28:1$
max voltage	$8\ (V)$
body length	$1.17\times10^{-1}\ (m)$
tail length	$1.27\times10^{-1}\ (m)$
body COM to pivot	$4.5\times10^{-2}\ (m)$
body mass	$1.6\times10^{-1}\ (kg)$
body COM inertia	$1.54\times10^{-4}\ (kgm^2)$
tail geartrain & motor	$1.11\times10^{-2}\ (kg)$
tail COM to pivot	$1.03\times10^{-1}\ (m)$
tail mass	$1.7\times10^{-2}\ (kg)$
tail COM inertia	$1.4\times10^{-5}\ (kgm^2)$

138 (mAh) batteries. Finally, a roll cage was fabricated to protect the electronics.

B. Tail Design

Our intent is to describe potential benefits to adding a tail to an existing platform; hence we constrained the design space to variables pertaining to the tail only, specifically motor power, gear ratio (input:output speed), and tail dimensions (length, mass, and moment of inertia). By recognizing that motor choice would be constrained by mass and packaging, we fixed motor torque and speed. We idealized the tail as a thin rod with a point mass at its end, eliminating tail MOI, and used the gear ratio that minimized maneuvering time for each combination of mass and length. Hence the final design space for our simple tail was two dimensional.

We used our dynamic model to evaluate maneuvering

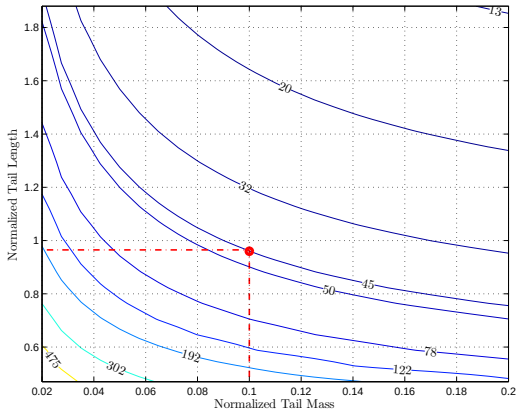

Fig. 7. Contour plot of absolute tail angle in degrees for the body to rotate 45° using a *tail* design with tail mass and length normalized against body mass and length respectively. The red dot indicates the design point for *Tailbot* where the desired relative mass of the tail is 10% and the desired absolute stroke of the tail is equivalent to the body stroke of 45°. As relative tail mass and length increase, the tail stroke decreases.

performance over a range of reasonable values for mass and length (2% to 20% body mass, one half to twice body length). To eliminate the effects of controller performance, we simulated aerial maneuvering with maximum open-loop torque. We measured the time required for the body to rotate 45°, along with the corresponding relative tail stroke required for the maneuver as shown in Fig. 7 when the links are initially 180° apart. For each combination of mass and length, we selected the gear ratio that yielded fastest rise time using a Nelder-Mead simplex direct search (*fmincon, MATLAB*). Optimal gear ratio varied significantly with tail geometry, from $16:1$ in the lower left corner of the design space of Fig. 5, to $90:1$ in the upper right. Both rise time and tail stroke were sensitive to changes in mass and length; in general, increasing either resulted in decreases in both rise time and required tail stroke.

The actual constraints on mass and length for a mobile robot in the field would be greatly task- and platform-dependent. While a climbing robot may prioritize low weight, a vehicle meant for tight spaces or rough terrain may require a shorter tail. In practice, tail stroke will be limited by the physical dimensions of the body. In this case, stroke may be used as a third constraint - the maximum allowable tail stroke for desired body stroke will yield a locus of points in the relative mass-length plane as shown in Fig. 7. Given the lack of real performance constraints in our robot, we chose to fix tail mass to 10% of body mass, and to inspire relative stroke requirements from the agamas, which on average use a relative tail stroke of two times body stroke (ie, absolute body and tail stroke will be roughly equal for small rotations). These two constraints lead to a robot tail length (with point mass at tip) of 10.3 (cm), about $0.9X$ body length. Our chosen tail geometry results in a predicted open loop rise time of 0.033 (s). Optimal gear ratio was about $60:1$. In the parameter range chosen, performance was relatively insensitive to design changes. Increasing tail length by 10% would decrease rise time 2% and tail stroke by 14%; increasing tail mass 10% would decrease rise time 1% and tail stroke 6%. In general the quadratic dependence of inertial loads on length results in more sensitivity to length change than mass change.

Due to space constraints on our existing platform, we were unable to accommodate the ideal gear ratio for the tail motor; we instead used a ratio of $17:1$. While our simulation assumed a massless rod, the actual tail's mass is 17 (g) (10% body mass) with rod and coupling, has an MOI of $1.4\times10^{-5}\ (kgm^2)$, and an overall length of 12.2 (cm) ($1.05X$ body length) as listed in Table I. These concessions result in slightly reduced performance; the model predicts a relative tail stroke of 47° and estimates the robot will need 0.05 (s) to complete the maneuver. The agamas in [8] had tails that weighted about 20% body mass, and were $1.3X$ body length on average. While lizard tails are roughly conical, we recognize that animal morphology is subject to a variety of other constraints, including development, musculature, and the multi-functional nature of tails. With the inclusion of the actuator (geartrain and motor), which

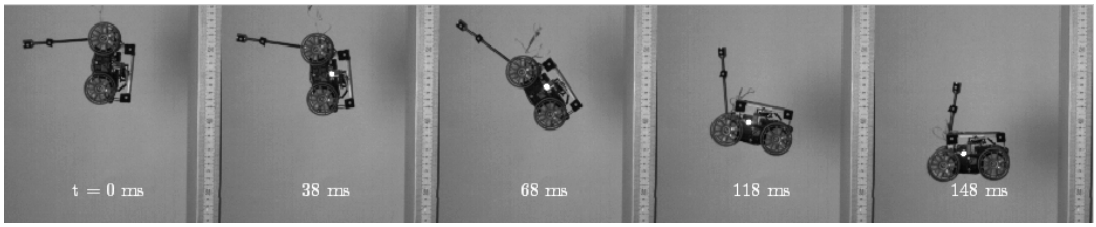

Fig. 8. Representative plot of a zero net angular momentum maneuver where the body was able to orient itself 90° from its initial condition in 0.138 (s). Shown in Exp. 1 in the supplemental video.

was placed on the body, the total mass to add a tail was 28 (g) or 18.7% of the body without actuator. Hence, while our engineered tail yields similar kinematic performance to that of the natural system, our design uses slightly less mass but 19% less overall length relative to body.

C. Sensing and Feedback Control

Since there is only one actuator for two DOF, the system is underactuated and the angle of both body and tail cannot be controlled simultaneously. At this stage, the orientation of the body will be deemed most important; hence we ignore tail angle and simply close the loop on body angle. In the future we can extend actuation to more degrees of freedom and use the tail angle information in the control scheme.

Over short time scales, the body angle can be accurately estimated from a gyroscope, but integration drift will accumulate error over time. Alternatively, an accelerometer can estimate orientation from the angle of the gravity vector with respect to body-fixed axes, but this estimate is sensitive to other accelerations and is not available during free fall. We devised a time varying complementary filtering (TVCF) method, which is discussed in [30] to combine these measurements and robustly estimate the instantaneous body angle. We collected kinematic data at 500 frames-per-second (fps) with a high speed camera (*HS1, Fastec Imaging*) and compared actual body angle to the estimate from the TVCF method. Results show that the method achieved a root-mean-square (RMS) error of less than 10°.

As a first approach to an active tail controller, we implemented a proportional-derivative (PD) controller based on the sensor fusion estimate of the body angle. The input to the controller was the desired body angle, $_{ref}$. The gains were manually tuned to produce acceptable rise time and settling time performance given a step signal at $_{ref}$. The controller was unaware of tail angle, except for limit switches that prevented the motor from applying torque against the tail's bump stops. We found this simple controller sufficient for the rapid, gross maneuvers of interest in dynamic terrestrial locomotion. However, extending the tail design to enable rotations in other axes will demand use of more sophisticated control schemes, such as those proposed in [12], [31], [32].

IV. Experimental Results

A. Experimental Methods

We evaluated the effectiveness of our active tail by observing the robot's behavior in three simple representations of locomotory challenges: a fall, a large perturbation, and a transition between surfaces of greatly differing slopes. For each of the following trials, the robot program was initiated wirelessly from a host computer. Kinematics were captured by both the onboard sensors and by a high speed camera at 500 (fps). Retro-reflective dots surrounded with black felt provided high-contrast markers for use with auto-digitizing software (*ProAnalyst, Xcitex Inc.*); angles and segment angular momentum were calculated with custom software (*MATLAB, Mathworks Inc.*).

For all experiments, the trials were repeated five times; measurements are reported as (mean $\pm$ one standard deviation). For the following simulation verification and falling experiments we ensured that no initial angular momentum was imparted to the system by releasing the robot from rest by a string. The specified controller was triggered when free fall was detected by monitoring the magnitude of the total acceleration.

B. Simulation Verification

To verify the model's predictive ability, we performed a free-fall test at maximum control effort and measured the time and tail stroke required to reorient the body 45°. The observed absolute tail stroke was (49 ± 2°), which was only 2° larger than the model-predicted value. The difference in stroke may be due to error in the method of determining MOI. The time to move the body to 45° was (0.064 ± 0.0026 (s)). The increase in time from the predicted 0.05 (s) can be attributed to the unmodeled friction in the system and error in the measurements of the maximum supply voltage, stall torque and no-load angular velocity of the DC motor.

C. Falling

Surviving falls remains a great challenge for climbing robots. When substrate contact is lost and unrecoverable, the ability to reorient and land on energy-absorbing limbs could be critical to avoid damage to the robot [33]. Roll cages have been shown to protect sensitive parts during falls [34], but increase overall size and may decrease mobility.

1) Pure Fall: To test the ability of *Tailbot* to rapidly reorient itself in a fall with a zero net angular momentum turn, the feedback controller was implemented with $_{ref} = 0$° and triggered at the detection of free-fall. We suspended the robot nose-down, allowing the tail to hang passively, and released the robot. *Tailbot* righted itself in about one body length of drop distance, and held the desired orientation until impact.

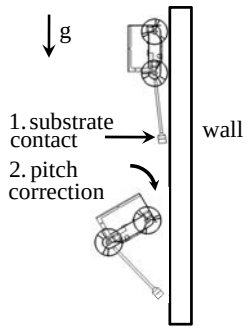

Fig. 9. Diagram of controlled body angle correction after falling from a wall.

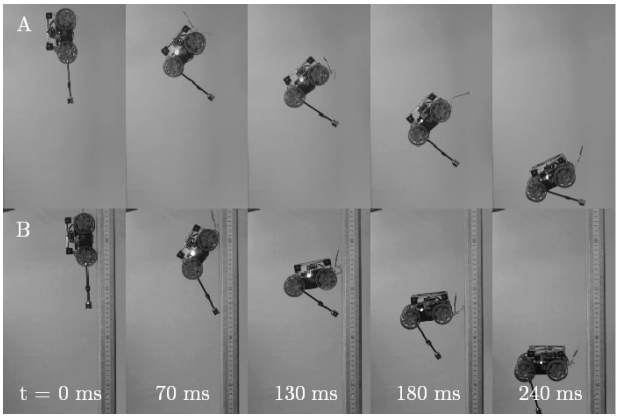

Fig. 10. A. The robot attempts to regulate the body angle, but is unable to do so due to tail saturation. B. When the robot is able to contact the wall and inject angular momentum into the system, saturation is avoided. With enough falling distance the tail will rotate enough to avoid being landed upon.

The rise time for this maneuver was $(0.138 \pm 1.09\ (s))$. A representative trial is shown in Fig. 8.

2) Falling from a Wall: While *Tailbot* can self-right from the initial orientation in Fig. 8, in a practical setting the tail would likely be held approximately parallel to the body, leaving less than 135° of available tail stroke for inertial maneuvering. In the previous section, the tail needed over 180° of relative stroke to rotate the body 90°, indicating that tail stroke saturation would prevent complete reorientation. Further, the wall itself may interfere with righting. To examine these issues, we dropped the robot in a parallel configuration both against a wall and in free space and compared righting performance. Again, the feedback controller initiated on free fall with $_{ref} = 0^\circ$. A representative sequence for each trial is shown in Fig. 10.

As predicted, the robot in open space was unable to fully regulate the body angle due to the physical constraint on tail stroke; the tail rotated a relative $(117.9 \pm 6.3^\circ)$ and hit the bump stop, which resulted in a maximum body angle stroke of only $(54.3 \pm 4.1^\circ)$. When the fall occurred from the wall, both the tail and the front wheel contacted the wall during the maneuver (Fig. 9). The contact force from the tail tip imparted net angular momentum to the robot, enabling complete reorientation without saturation. However, the angular momentum remained during the entire course of the fall, requiring the controller to continuously rotate the tail to regulate body angle. Given enough falling distance, this effect would further allow the tail to rotate away from the underbelly of the robot when landing, however a future tail design should incorporate a selective flexibility at the tail-base if landing on the tail became unavoidable. In this case, the ability to contact the substrate to generate angular momentum, and the ability to store angular momentum in an inertial structure were both required to complete the maneuver. When the mass was removed from the tail tip, the robot overshot horizontal and continued pitching forward. In less than 2.5 body lengths of drop distance, the robot was pointed straight down.

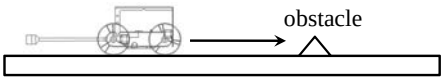

Fig. 11. Diagram of single obstacle.

D. Perturbation During Terrestrial Locomotion

To test the ability of the active tail to help mitigate perturbations in a rapid locomotory task, we drove *Tailbot* along a track with a single obstacle placed in the path as shown in Fig. 11. The geometry of the obstacle and speed of the robot was chosen to elicit a perturbation that exceeded the stability boundary of *Tailbot* without a tail.

We drove the robot into the obstacle with the same forward speed for each of three different cases: *Tailbot* without tail, *Tailbot* with a passive tail (controller off), and *Tailbot* with an active tail using the PD feedback controller. The feedback controller was implemented with $_{ref} = 0^\circ$ during the entire trial.

The maximum body angle due to the perturbation was recorded for each case. A representative sequence of these trials is shown in Fig. 12 on the next page. From row A, the tailless robot failed in every trial. From row B, the robot with a passive tail was able to overcome the obstacle, but the maximum measured body angle was large $(67 \pm 6.9^\circ)$. With the feedback controller on as shown in row C, the maximum body angle was reduced by over half $(28 \pm 2.8^\circ)$. During this trial the tail was able to compensate for a large perturbation even though the tail made contact with the substrate during the perturbation, since the contact and inertial torque occur in the same direction.

E. Completing Transitions

Figure 14 shows a task to evaluate the ability of *Tailbot* to transition between surfaces of significantly different slopes using an inertial maneuver. We drove the robot off a horizontal surface towards an inclined surface. On horizontal ground we set the reference angle $_{ref} = 0^\circ$; when the robot left the surface we switched the reference angle to $_{ref} = 45^\circ$, to achieve the proper landing angle. For simplicity, the switching was accomplished with feedforward timing, but in real applications, switching could be facilitated by

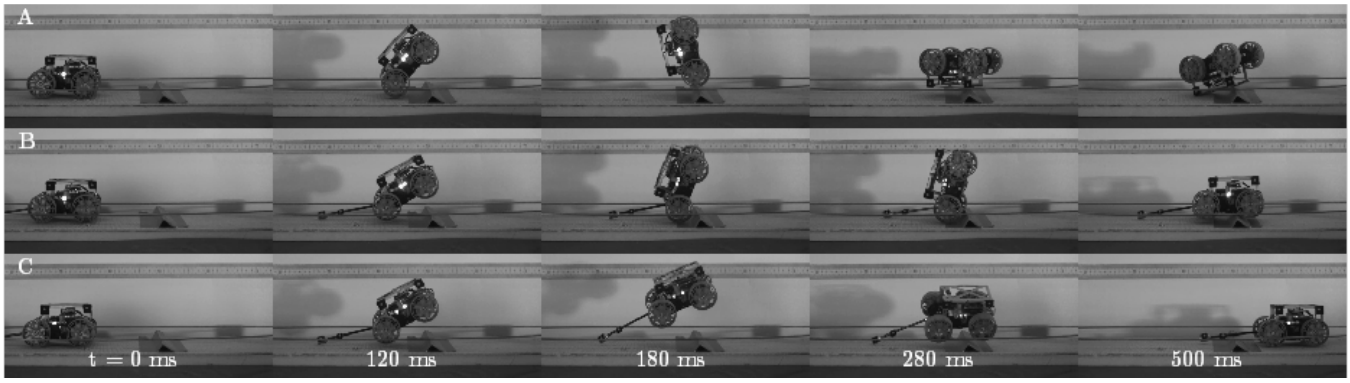

Fig. 12. A. With no tail the robot catastrophically fails when traversing the obstacle. B. When the tail is passive the robot succeeds in traversing the obstacle, but the peak body angle of the robot is large ($> 60°$). C. When the body angle is controlled by the tail then the robot is able to successfully traverse the obstacle with much less peak body angle ($< 30°$).

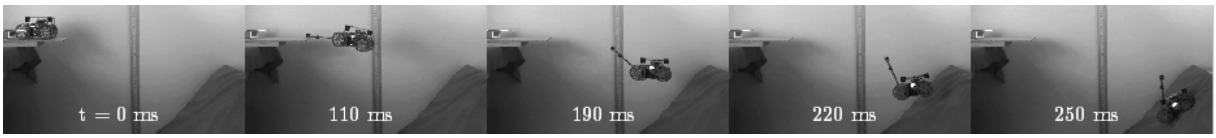

Fig. 13. Representative trial demonstrating a rapid transition task which occurs in 0.25 (s).

visual servoing or other high-level control systems. Due to a moment resulting from gravity as the robot rolls off the horizontal platform, a disturbance was introduced into the system in the form of pitch-axis angular momentum.

In all trials, the robot initially pitched down due to the perturbation before swinging the tail and directing the body to match the wall angle and landing safely. By combining visual servoing with an inertial tail, a robot could use short aerial phases to smooth the transitions between uneven surfaces.

V. CONCLUSIONS AND FUTURE WORKS

We have shown that a robot with an appendage designed for both inertial and contact torques could enable rapid air-reorientation, improve fall survivability, and increase mobility and stability over difficult terrain. Our robot can reorient 90° in one body length of vertical fall, survive perturbations that would flip an tailless robot, and effect rapid angle changes to smooth transitions between surfaces. Our bio-inspired tail-like design has several advantages over alternative technologies such as reaction wheels: low weight, high rotational inertia, and the capability to apply external torques via substrate contact. We found that contact torques and inertial torques can be modulated with the same simple controller to produce predictable, directed body rotation.

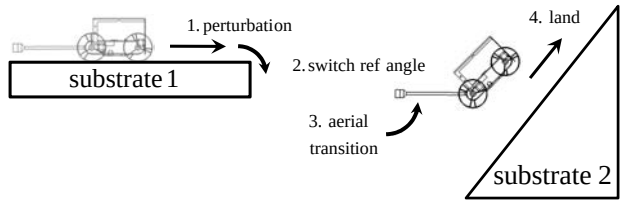

Fig. 14. Diagram of transition task from flat substrate to inclined wall.

Future work will focus on extending these results to three-axis rotations. Observations in lizards indicate that by adding a yaw DOF to the tail, we can effect body rotations in not only yaw, but roll as well. We will also investigate the possibility of dynamically changing the flexibility or MOI of the tail to reduce the problem of limited tail stroke. Addition of a tail to the next generation of dynamic legged robots could increase their ability to perform in environments too inaccessible or dangerous for humans, such as in search-and-rescue missions.

VI. ACKNOWLEDGMENTS

The authors gratefully acknowledge the Center for Interdisciplinary Bio-inspiration in Education and Research (CiBER), Mr. Sumio Sugita, Ms. Debbie Li, Mr. Jon Beard, Prof. Oliver O'Reilly, Prof. Ron Fearing, and Prof. Hari Dharan for their advice and contributions to the modeling, experimentation, and construction of *Tailbot*.

VII. APPENDIX

Equations (6) and (7) display the contents of $\mathbf{f}(\mathbf{x})$ and $\mathbf{g}(\mathbf{x})$. The distance from the pivot to the COM of each link is l_i, which is equal to magnitude of $_i$.

REFERENCES

[1] J. Casper and R. R. Murphy, "Human-robot interactions during the robot-assisted urban search and rescue response at the world trade center," *Systems, Man, and Cybernetics, Part B: Cybernetics, IEEE Transactions on*, vol. 33, no. 3, pp. 367–385, 2003.

[2] U. Saranli, M. Buehler, and D. E. Koditschek, "Rhex: A simple and highly mobile hexapod robot," *The International Journal of Robotics Research*, vol. 20, no. 7, pp. 616–631, 2001.

[3] P. Birkmeyer, K. Peterson, and R. S. Fearing, "Dash: A dynamic 16g hexapedal robot," in *Intelligent Robots and Systems, 2009. IROS 2009. IEEE/RSJ International Conference on*, 2009, pp. 2683–2689.

$$\mathbf{f}(\mathbf{x}) = \begin{bmatrix} \dot{\theta}_1 \\ \frac{\frac{1}{2}l_1^2 l_2^2 m_1^2 m_2^2 \dot{\theta}_1^2 \sin(2(\theta_1-\theta_2)) - (l_2^2 m_1 m_2 + I_2(m_1+m_2)) l_1 l_2 m_1 m_2 \dot{\theta}_2^2 \sin(\theta_1-\theta_2)}{l_1^2 l_2^2 m_1^2 m_2^2 \cos(\theta_1-\theta_2)^2 - (l_1^2 m_1 m_2 + I_1(m_1+m_2))(l_2^2 m_1 m_2 + I_2(m_1+m_2))} \\ \dot{\theta}_2 \\ -\frac{\frac{1}{2}l_1^2 l_2^2 m_1^2 m_2^2 \dot{\theta}_1^2 \sin(2(\theta_1-\theta_2)) + (l_1^2 m_1 m_2 + I_1(m_1+m_2)) l_1 l_2 m_1 m_2 \dot{\theta}_2^2 \sin(\theta_1-\theta_2)}{l_1^2 l_2^2 m_1^2 m_2^2 \cos(\theta_1-\theta_2)^2 - (l_1^2 m_1 m_2 + I_1(m_1+m_2))(l_2^2 m_1 m_2 + I_2(m_1+m_2))} \end{bmatrix} \tag{6}$$

$$\mathbf{g}(\mathbf{x}) = \begin{bmatrix} 0 \\ -\frac{(l_2^2 m_1 m_2 + I_2(m_1+m_2) - l_1 l_2 m_1 m_2 \cos(\theta_1-\theta_2))(m_1+m_2)}{l_1^2 l_2^2 m_1^2 m_2^2 \cos(\theta_1-\theta_2)^2 - (l_1^2 m_1 m_2 + I_1(m_1+m_2))(l_2^2 m_1 m_2 + I_2(m_1+m_2))} \\ 0 \\ \frac{(l_1^2 m_1 m_2 + I_1(m_1+m_2) - l_1 l_2 m_1 m_2 \cos(\theta_1-\theta_2))(m_1+m_2)}{l_1^2 l_2^2 m_1^2 m_2^2 \cos(\theta_1-\theta_2)^2 - (l_1^2 m_1 m_2 + I_1(m_1+m_2))(l_2^2 m_1 m_2 + I_2(m_1+m_2))} \end{bmatrix} \tag{7}$$

[4] M. J. Spenko, G. C. Haynes, J. A. Saunders, M. R. Cutkosky, A. A. Rizzi, R. J. Full, and D. E. Koditschek, "Biologically inspired climbing with a hexapedal robot," *Journal of Field Robotics*, vol. 25, no. 4-5, pp. 223–242, 2008.

[5] C. Menon, M. Murphy, and M. Sitti, "Gecko inspired surface climbing robots," in *Robotics and Biomimetics, 2004. ROBIO 2004. IEEE International Conference on*, 2004, pp. 431–436.

[6] A. T. Asbeck, S. Kim, M. R. Cutkosky, W. R. Provancher, and M. Lanzetta, "Scaling hard vertical surfaces with compliant microspine arrays," *The International Journal of Robotics Research*, vol. 25, no. 12, pp. 1165–1179, 2006.

[7] A. Jusufi, D. T. Kawano, T. Libby, and R. J. Full, "Righting and turning in mid-air using appendage inertia: reptile tails, analytical models and bio-inspired robots," *Bioinspiration & Biomimetics*, vol. 5, no. 4, p. 045001, 2010.

[8] T. Libby, E. Chang-Siu, and R. J. Full, "Dynamic stabilization of rapid transitions in a lizard and a robot with an active tail," *In Prep*, 2011.

[9] T. R. Kane and M. P. Scher, "A dynamical explanation of the falling cat phenomenon," *International Journal of Solids and Structures*, vol. 5, no. 7, pp. 663–666, 1969, doi: DOI: 10.1016/0020-7683(69)90086-9.

[10] R. Montgomery, "Guage theory of the falling cat," *M.J. Enos(Ed.), Dynamics and Control of Mechanical Systems, American Mathematical Society*, pp. 193–218, 1993.

[11] E. Papadopoulos, I. Fragkos, and I. Tortopidis, "On robot gymnastics planning with non-zero angular momentum," in *Robotics and Automation, 2007 IEEE International Conference on*, 2007, pp. 1443–1448.

[12] X. Xin, T. Mita, and M. Kaneda, "The posture control of a two-link free flying acrobot with initial angular momentum," *Automatic Control, IEEE Transactions on*, vol. 49, no. 7, pp. 1201–1206, 2004.

[13] A. Jusufi, D. I. Goldman, S. Revzen, and R. J. Full, "Active tails enhance arboreal acrobatics in geckos," *Proceedings of the National Academy of Sciences*, vol. 105, no. 11, pp. 4215–4219, 2008.

[14] E. Papadopoulos and S. Dubowsky, "On the nature of control algorithms for free-floating space manipulators," *Robotics and Automation, IEEE Transactions on*, vol. 7, no. 6, pp. 750–758, 1991.

[15] K. Yoshida and Y. Umetani, "Control of space free-flying robot," in *Decision and Control, 1990., Proceedings of the 29th IEEE Conference on*, 1990, pp. 97–102 vol.1.

[16] C. Fernandes, L. Gurvits, and L. Zexiang, "Attitude control of a space platform/manipulator system using internal motion," *The International Journal of Robotics Research*, vol. 13, no. 4, pp. 289–304, 1994.

[17] R. W. Longman, R. E. Lindbergt, and M. F. Zedd, "Satellite-mounted robot manipulators new kinematics and reaction moment compensation," *The International Journal of Robotics Research*, vol. 6, no. 3, pp. 87–103, 1987.

[18] F. Saito, T. Fukuda, and F. Arai, "Swing and locomotion control for two-link brachiation robot," in *Robotics and Automation, 1993. Proceedings., 1993 IEEE International Conference on*, 1993, pp. 719–724 vol.2.

[19] Z. Li and R. Montgomery, "Dynamics and optimal control of a legged robot in flight phase," in *Robotics and Automation, 1990. Proceedings., 1990 IEEE International Conference on*, 1990, pp. 1816–1821 vol.3.

[20] T. Rokusho, J. Lee, M. Yamakita, S. Hirano, and Z. W. Luo, "Landing control of acrobat robot by rhc -experimental evaluation," in *SICE-ICASE, 2006. International Joint Conference*, 2006, pp. 4808–4813.

[21] K. Yamafuji, T. Kawamura, K. Tanaka, and M. Feng, "Elucidation of twisting motion of a falling cat and realization of the cat-turn motion by a robot," *INTERNATIONAL SYMPOSIUM ON ROBOTICS*, vol. 30, pp. 527–534, 1999.

[22] L. Keo and M. Yamakita, "Controlling balancer and steering for bicycle stabilization," in *Intelligent Robots and Systems, 2009. IROS 2009. IEEE/RSJ International Conference on*, 2009, pp. 4541–4546.

[23] M. Yamakita and A. Utano, "Automatic control of bicycles with a balancer," in *Advanced Intelligent Mechatronics. Proceedings, 2005 IEEE/ASME International Conference on*, 2005, pp. 1245–1250.

[24] "Murata boy. http://www.murataboy.com/en/index.html," 2011.

[25] S. Floyd, T. Keegan, J. Palmisano, and M. Sitti, "A novel water running robot inspired by basilisk lizards," in *Intelligent Robots and Systems, 2006 IEEE/RSJ International Conference on*, 2006, pp. 5430–5436.

[26] M. D. Berkemeier and R. S. Fearing, "Control of a two-link robot to achieve sliding and hopping gaits," in *Robotics and Automation, 1992. Proceedings., 1992 IEEE International Conference on*, 1992, pp. 286–291 vol.1.

[27] T. Kohlsdorf, T. Garland, and C. A. Navas, "Limb and tail lengths in relation to substrate usage in tropidurus lizards," *Journal of Morphology*, vol. 248.2, pp. 151–164, 2001.

[28] T. W. Mather and M. Yim, "Modular configuration design for a controlled fall," in *Intelligent Robots and Systems, 2009. IROS 2009. IEEE/RSJ International Conference on*, 2009, pp. 5905–5910.

[29] J. J. Dowling, J. L. Durkin, and D. M. Andrews, "The uncertainty of the pendulum method for the determination of the moment of inertia," *Medical Engineering & Physics*, vol. 28, no. 8, pp. 837–841, 2006, doi: DOI: 10.1016/j.medengphy.2005.11.007.

[30] E. Chang-Siu, K. Kong, and M. Tomizuka, "Time-varying complementary filtering for attitude estimation," *In Prep*, 2011.

[31] Z. Weng and H. Nishimura, "Final-state control of a two-link cat robot," *Advanced Robotics*, vol. 16, pp. 325–343, 2002, doi:10.1163/15685530260174511.

[32] Y. Yi-Ling, P. C. P. Chao, and S. Cheng-Kuo, "Landing posture control via trajectory planning for a generalized twin-body system," in *Autonomous Robots and Agents, 2009. ICARA 2009. 4th International Conference on*, 2009, pp. 97–102.

[33] M. C. Jonathan and C. A. Ronald, "Survival of falling robots," J. W. William and H. C. Wendell, Eds., vol. 1613. SPIE, 1992, pp. 91–102, mobile Robots VI 1.

[34] M. Kovac, M. Schlegel, J. C. Zufferey, and D. Floreano, "A miniature jumping robot with self-recovery capabilities," in *Intelligent Robots and Systems, 2009. IROS 2009. IEEE/RSJ International Conference on*, 2009, pp. 583–588.